

A Framework for Synthetic Power System Dynamics

Anna Büttner, Anton Plietzsch, Mehrnaz Anvari and Frank Hellmann

Potsdam-Institute for Climate Impact Research

November 2022

Abstract. Information on power grids is confidential and thus real data is often inaccessible. This necessitates the use of synthetic power grid models in research. So far the models used, for example, in machine learning had to be very simple and homogeneous to produce large ensembles of robust grids. We present a modular framework to generate synthetic power grids that considers the heterogeneity of real power grid dynamics but remains simple and tractable. This enables the generation of large sets of synthetic grids for a wide range of applications. We also include the major drivers of fluctuations on short-time scales. The synthetic grids generated are robust and show good synchronization under all evaluated scenarios, as should be expected for realistic power grids. This opens the door to future research that studies grids under severe stress due to extreme events which could lead to destabilization and black-outs. A software package that includes an efficient Julia implementation of the framework is released as a companion to the paper.

1. Introduction

Synthetic power grids have become an important tool for studying the dynamics of power systems. Traditionally, most dynamical simulation studies in the engineering literature were performed using benchmark test cases, such as the "New England" IEEE 39-Bus System [1] or the IEEE Reliability Test System-1996 [2]. The advantage of this approach is that models and parameters can be specified in great detail and the test cases are therefore highly realistic. Further, the use of standardized benchmark test cases guarantees a certain comparability of different dynamic models and analytical methods. However, for many emerging research questions this approach can be quite limiting and the use of automatically generated synthetic grid models might be beneficial. This is for instance the case when the power system in a specific region should be studied but the detailed topology and parameters of the real grid are not publicly accessible. Often there is enough data or knowledge available to generate a synthetic grid that resembles the main properties of a real grid to a reasonable degree. An example is the algorithm by Birchfield et al. [3, 4] that generates realistic transmission network topologies from spatial load distributions based on geographic population data. The algorithm is expanded in [5] to also enable transient stability analysis of the synthetic

power grids. Besides the transmission system, synthetic grids are also required for studying mid- and low-voltage grids as their exact structure is often unknown [6]. For German medium and low-voltage grids, the *DingO* model [7] is an extensive and well-documented option to generate topologies [7] and supply and demand distributions [?]. *DingO* is part of the larger research project *open eGo* and is an open-source software that uses freely available data.

Another important use case for synthetic power grid models is to generate large data sets of synthetic test cases that can be used to investigate the system dynamics with methods of machine learning [8, 9]. A number of studies have shown that the network topology of grids has a direct influence on their dynamic stability [10–12]. However, most of these studies are based on very simplistic component models and unrealistically homogeneous parameters. Graph-Neural-Networks have been shown to be a powerful method that could potentially extend these stability analyses to more realistic power grid models [9, 13, 14]. The training of such neural networks requires large data sets of realistic grids, that are for example generated by a synthetic grid model.

Finally, synthetic grid models will be crucially important for the investigation of dynamic effects of future power grids. Within the next decades, the power system will undergo a fundamental transformation as new transmission infrastructure is built and conventional machines are replaced by renewable energy sources (RES). A major challenge is that the exact dynamical behavior of generation units is widely unknown as renewable generation units are connected to the grid via inverters with various control schemes. In order to maintain stability in such inverter-based grids, a certain share of these controls have to be grid-forming. Today, most RES are still equipped with grid-following control schemes and hence, there is a lack of practical knowledge on the collective dynamical behavior of a large number of grid-forming generation units. It is therefore of great importance to do simulation studies of these systems to ensure that new technology being integrated into the grid does not lead to unexpected collective effects and blackouts [15]. Unfortunately, there is a lack of both benchmark test cases as well as synthetic power grid models for studying such inverter-based grids.

In this paper, we present a modular framework for generating synthetic grids that are suited for dynamic power system studies. We give an overview of all necessary steps from the generation of grid topologies, to the definition and parametrization of component models and the calculation of the steady state. The paper is accompanied by a software repository that provides an implementation of all algorithms described in this paper. Our approach is modular in the sense that users can easily adapt each step in the grid generation process to their own needs, e.g. by providing their own specific grid topologies or by using different dynamic models for the generating units in the system. We focus on extra high voltage (EHV) level transmission grids, which in the continental European transmission grid includes the 380 kV–400 kV and the 220 kV voltage levels. Collective dynamical effects are traditionally studied in the highest grid layer [16], which is why we can rely on a comprehensive foundation there. In principle, the approach presented extends to all grid layers though.

The framework is designed to be capable of efficiently generating large numbers of synthetic grids with very limited input data. At the same time the component models and parameters have a comparatively high level of realism: Generator and inverter models feature voltage dynamics, the active power production and demand are heterogeneous and the parametrization of line admittances is according to data of the German transmission grid. The framework is therefore well-suited for applying machine learning methods, e.g. to predict dynamical stability from the structural properties of the grid.

Another important feature is the possibility to model power grids with high shares of inverter-based generation units. For this, we bypass the problem that the exact dynamical models of such systems are still uncertain by using a technology and control scheme neutral model [17] that has been shown to reproduce the behavior of a large class of different inverter controls. However, we also point out open research questions for improving the modeling of future power grids.

2. Synthetic Power Grid Framework

The modular framework introduced in this paper adopts the following structure: First, a topology or network structure for the synthetic power grid is generated. Then active power set points for the nodes in the network are defined. The next step is to specify the node and line models in order to populate the networks with dynamics. Then an operation point, that fulfills certain stability criteria, is determined. In the last step, we validate the synthetic grids and assure that the dynamic network properties are similar to those of real power grids that are carefully planned.

For the analysis of the resulting grids, we also provide stochastic models that characterize fluctuations processes that are typical at the timescale of interest.

In the following, we will describe the default settings of each step of the algorithm. As the framework is modular each step can be switched out by another approach as long as it adheres to the general structure.

Most of the steps presented here have been used in research projects before, however they are now, for the first time, combined as a comprehensive package that is available for further research. Particularly, it is the first step towards a synthetic model of future power grids with high integration of RES. Each section contains a summary of a step in the framework as well as a critical analysis of the state-of-the-art. In the respective sections, we give an outlook and show which additional work could be done to improve the model, particularly for the representation of future power grids.

2.1. Grid Topology

The default topologies in our framework are generated using the random growth algorithm introduced in [18]. We choose this model as it is conceptually straightforward to generate a large number of interesting and plausible topologies and as it has

little computational complexity, which is convenient for generating large ensembles of synthetic test cases. However, it is at the conceptual end of the synthetic grid spectrum. If the interest is to study dynamics on more realistic topologies, other models should be employed.

The algorithm of [18] generates synthetic networks that resemble EHV real-world power grids with respect to the exponentially decaying degree distribution and the mean degree. The algorithm includes first an initialization phase, where a spatially embedded minimum spanning tree is generated, and then a growth phase. The growth phase includes a heuristic target function for the trade-off between the total line length, which determines the costs, and the smallest number of edges that would need to be removed to disconnect the grid into two parts, which influences the redundancy.

The default parameters of the growth algorithm have been set to $[N_0, p, q, r, s] = [1, 1/5, 3/10, 1/3, 1/10]$, as employed in [12], where N_0 is the initial number of nodes in the minimum spanning tree, p , q are the probabilities for generating a new redundant line, s is the probability of splitting an existing line, and r is the exponent for the trade-off between redundancy and cost.

Since distribution grids typically exhibit rather different network structures (mostly radial and ring topologies [7]) these parameters have to be adapted when the growth algorithm should be used for modeling lower voltage levels.

For the default step, we assume that there is no correlation between the grid topology and the positioning of generation units in future grids. We thus assume that the transmission system topology will remain very similar to today, even if the position of generation units will be correlated to the renewable energy potentials and the location of generation thus changes. This is not entirely realistic and future studies should consider that the grid will be expanded and adapted to the new supply sources. However, such changes are expensive and time consuming [19] and thus likely to be limited. To properly incorporate these aspects a synthetic geographical model, potentially incorporating economic optimization, such as [20] is needed.

2.2. Active Power Distribution

In order to correctly represent the dynamics of the power grid, a realistic distribution of power in the grid is required. For this purpose the *ELMOD-DE* [21] data set, an open-source spatially distributed, nodal dispatch model for the German transmission system is consulted. Following [22], which also analyses the data set, we examine the net power ΔP at each node given in the data set.

The *ELMOD* data set includes a time series for the total demand P_{tot} in all of Germany. The demand is distributed to the individual nodes by introducing the nodal load share ls_m which specifies the proportion of the consumption of a node m from the total demand P_{tot} . It is distinguished between two different types of load scenarios, off-peak and on-peak. Egerer et. al. [21] defines on-peak and off-peak as the highest and lowest load level meaning the maximum and minimum of P_{tot} respectively. The data set gives the

load shares ls_m for both scenarios the off-peak and on-peak. In the following, we will always work with the off-peak scenario. The consumption at a node $P_{con,m}$ is then given by:

$$P_{con,m} = P_{tot} \cdot ls_m. \quad (1)$$

The *ELMOD* data set includes the installed capacity for each generation unit c_j , which is the maximum power output the unit j can produce. As multiple power plants can be connected to a single node, the nodal capacity C_m is given by the sum of all capacities at the node $C_m = \sum_j c_j$. Typically, the full capacity of a generation unit is not available. In addition to the approach by Taher et al. [22], we also include the availability factors a^{tech} for each technology during the off-peak scenario. The nodal availability A_m is then given by:

$$A_m = \sum_j c_j \cdot a^{tech}. \quad (2)$$

The total available power is defined as $A_{tot} = \sum_m A_m$. As there is no data about how much power each node generates at a given time point we follow the approach given in [22] and reduce the nodal availability A_m by the factor $x = \frac{P_{tot}}{A_{tot}}$, such that generation and consumption are balanced. The nodal generation $P_{gen,m}$ is thus given by: $P_{gen,m} = A_m \cdot x$. Finally, we can define the net nodal power ΔP_m as:

$$\Delta P_m = P_{gen,m} - P_{con,m}. \quad (3)$$

Figure 1 shows a histogram of ΔP_m . It can be seen that the distribution is bimodal, asymmetric and that the power generation is heavy-tailed. The heavy tail in the distribution of the power distribution can be explained by the structure of today's power grid where the power is mostly produced by a smaller number of large generators. In the *ELMOD* data set 301 nodes are classified as net consumers, while only 137 are net generators. For a future RES heavy scenario one can replace the capacities and availabilities above with a model for the deployment of wind and solar renewable resources.

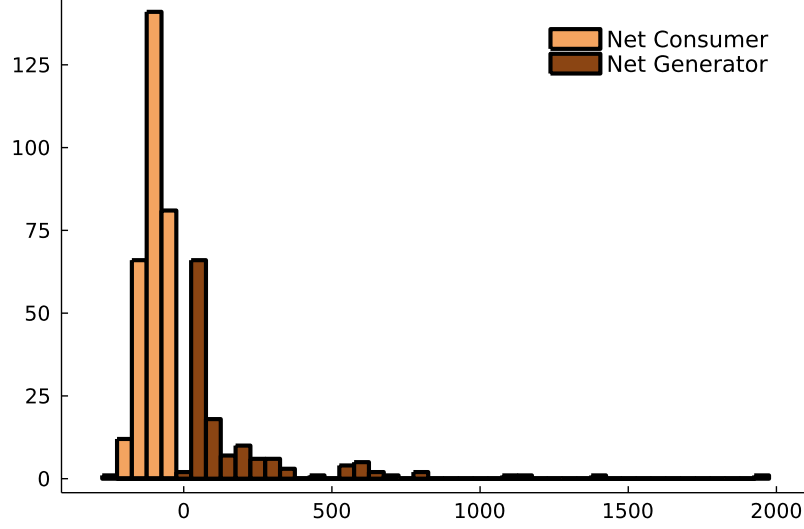


Figure 1: Histograms of the net nodal generation and consumption in the *ELMOD-DE* [21] data set during the off-peak scenario. The distribution is bimodal and asymmetric. The power generation shows a heavy tail.

Following [22] the active power P of each node is sampled from a bimodal distribution, given by:

$$p(P) = \frac{1}{2\sigma\sqrt{2\pi}} \left(\exp \frac{(P - P_0)^2}{2\sigma^2} + \exp \frac{(P + P_0)^2}{2\sigma^2} \right) \quad (4)$$

in this work we will use $P_0 = \overline{\Delta P_{380}} \approx 131$ MW.

The topologies used here, mimic the extra high voltage 380 kV transmission grids. All following calculations are performed in a Per-Unit-System (p.u.), meaning that an appropriate base power P_{base} and base voltage V_{base} have to be chosen. As this work only examines the highest voltage layer of the grid the base voltage is simply chosen as $V_{base} = 380$ kV. To define the base power for the 380 kV level we extract all nodes that are connected to 380 kV lines and calculate the mean $\overline{\Delta P_{380}} \approx 131$ MW. Based on the available data, we choose $P_{base} = 100$ MW as the base power for the synthetic power grids.

The *ELMOD* data set represents the current load and capacity distribution, which means that renewables are still in the minority. The analysis shown here is suitable for the distribution of active power in synthetic grids which should represent the status quo as most buses are either generation heavy or load heavy. For this work, we will adopt the bimodal model which was introduced in [22]. How this distribution will change due to the increasing share of RES but also changing consumption remains an open research question. A promising possibility is to base the distribution of active power supply on the renewable potentials of geographical areas. For this purpose, established software packages, such as atlite [23], could be consulted. For the consumption side, new sectors with additional loads will be connected to the electric grid, for example, electric cars or hydrogen production.

Furthermore, it should also be taken into account that the set points for the power change in the grid over time due to the evolution of the demand over the day and year. Typically these set points are updated every 15 minutes based on a cost optimization procedure. It would be valuable to study a grid and its dynamics under different load scenarios. Moreover, the demand is not constant between two dispatch times, but fluctuates, for example, studied in [24]. In section 3.2 we will apply the model for realistic demand fluctuations, which has been derived in [24], to our power grids. Future work could also consider that the generation is typically distributed via an cost optimization approach.

2.3. Power Grid Model

On the most abstract level, we will mathematically describe power grids as systems of differential-algebraic equations (DAEs). The constraints mostly appear in the load models. Explicit DAEs are defined as:

$$\dot{x} = f(x, y) \quad (5)$$

$$0 = g(x, y) \quad (6)$$

where equation (5) and (6) represent the differential and algebraic equations respectively. The vector x holds the differential variables, whose derivatives appear in the DAE, while the vector y gives the algebraic variables, whose derivatives do not appear.

The specific models for the nodes and lines as well as for the networks are introduced in the following sections.

2.3.1. Node Models Our synthetic grids will consist of grid-forming components, for example, power plants and novel types of inverters that contribute to grid stability and components without grid-forming capabilities, such as loads or grid-following inverters, that have to rely on an already stable grid. For this work, we have decided to use elementary nodal models to depict components with and without grid-forming abilities that are able to cover a large range of dynamical actors.

In this work, PQ-buses [25] are used to represent the components without grid-forming behavior. The PQ-bus locally fixes the active and reactive power of node m :

$$0 = (P_{set,m} + iQ_{set,m}) - u_m \cdot i_m^* \quad (7)$$

where $P_{set,m}$ and $Q_{set,m}$ are the active and reactive power set points of the node, and u_m and i_m are respectively the voltage and current of node m . The model can depict either loads or sub-networks of consumers and renewable energy producers who are connected to the grid via grid-following inverters. The PQ-bus (7) is a constraint equation as given in equation (6) and forces us to use the DAE description of the power grids.

To represent grid-forming components we use the normal-form, a technology-neutral model for grid-forming actors, that has been introduced in [17]. The normal form captures the most important nonlinearities of grid-forming components. Various models

of grid-forming components, such as droop-controlled inverters [26] and synchronous machine models [27], have been mapped to the normal form. The normal form has been validated by numerical simulations and lab measurements of a grid-forming inverter so far. A normal form at node m with a single internal variable, the frequency ω_m , is given by:

$$\begin{aligned} v_m^2 &= u_m u_m^* \\ \dot{\omega}_m &= A^{x,m} + B^{x,m} \delta\omega_m + C^{x,m} \delta v_m^2 + G^{x,m} \delta P_m + H^{x,m} \delta Q_m \\ \frac{\dot{u}_m}{u_m} &= A^{u,m} + B^{u,m} \delta\omega_m + C^{u,m} \delta v_m^2 + G^{u,m} \delta P_m + H^{u,m} \delta Q_k \end{aligned} \quad (8)$$

where u_m is the complex voltage. δP_m and δQ_m represent the difference of the active and reactive power to the set-points. δv_m^2 is the difference of the squared voltage magnitude v_m^2 to the squared voltage set-point. The other coefficients are the modeling parameters that capture all the differences between the various models the normal form can represent. The parameters $A^{x,m}$ and $A^{u,m}$ are zero when the system is, as in our case, defined in the co-rotating reference frame. In the normal form, all differences between the two models are absorbed in the parametrization.

The free parameters for the normal form can be gathered by approximating other models, moreover, it is also possible to derive them from experimental data, which has also been performed in [17] for a specific type of inverter in a lab. For the example provided in this work we will use a normal form approximation of a droop-controlled inverter [26] whose parameters can be derived analytically.

The exact ability of the normal form to cover all needed dynamics is subject of current research. We expect that the normal form captures the dynamics of sub-networks which include grid-forming components as well. Future work will include measurements on different types of inverters and deriving the parameters of the normal form from the data. This is a crucial step to study the dynamics and stability of realistic future power grids, which will consist of a variety of interacting grid-forming inverters.

In addition to the models for grid-forming and following components we introduce a slack bus [25] into the synthetic power grid model. The slack bus locally fixes the voltage u_m of node m :

$$0 = u_{set,m} - u_m. \quad (9)$$

where $u_{set,m}$ is the set point voltage. The voltage magnitude $|u_{set,m}|$ of the slack is typically set to 1 p.u. and its voltage angle is $\phi_m = 0^\circ$. The slack bus is used as the reference for all other buses in the system. While solving the load flow problem, the active and reactive power of the slack are free to change to compensate for the power imbalance in the network. Therefore it is assumed that the slack bus has a large amount of energy stored which can be released quickly. The slack bus is typically considered to be a large power plant or battery, a connection point to a higher grid layer, or another part of the power system which is not modeled explicitly.

2.3.2. Line Model For this work, the Pi-Model, see for example [28], is used. In the Pi-Model the impedance $Z_{km} = \frac{1}{Y_{km}}$ is placed in the center of the line. The capacitance between the line and the ground is also taken into account by introducing the shunt admittance $Y_{sh,km}$ which is placed, in parallel, at both ends of the line. The current on the lines connecting node k and m is then given by [28]:

$$I_{km} = Y_{km}(U_k - U_m) + Y_{sh,km}U_k \quad (10)$$

$$I_{mk} = Y_{km}(U_m - U_k) + Y_{sh,km}U_m \quad (11)$$

where Y_{km} is the impedance of a line connecting node k and m and U_k and U_m are the complex nodal voltages. The impedance Y_{km} and shunts are calculated according to the *dena* model of standard 380 kV overhead power lines [29] given in table 1. The reactance X is specified for the nominal frequency of 50 Hz, which is why we use a static line model here. The admittance Y is calculated according to:

$$k_c = \frac{cables}{cables_{typical}} \quad (12)$$

$$k_w = \frac{wires}{wires_{typical}} \quad (13)$$

$$Y_{km} = \frac{k_c k_w}{R + jX} l_{km} \quad (14)$$

$$Y_{sh,km} = \frac{-(j\omega C_{sh})k_c k_w}{2} l_{km} \quad (15)$$

where l_{km} is the line length in kilometers. For consistency, we fix the grid frequency ω , in the shunt capacitance $Y_{sh,km}$, to the nominal frequency. The coefficients k_c and k_w define the ratio between the typical number of cables $cables_{typical}$ and wires $wires_{typical}$ and the actual numbers in the line [30]. The typical numbers of cables and wires is 3 and 4 respectively for transmission lines in the 380 level in Germany [30]. In the default version of the algorithm, we assume that all transmission lines have the typical number of cables and wires. Section 2.5.4 introduces an additional step in the algorithm where probabilistic power flow scenarios are considered and the line capacities are increased, by adding a new cable to the existing line mk , if a load scenario leads to an overload in line mk . This ensures that the line parameters are well-suited for the load flow used.

Voltage level	R [Ω /km]	X [Ω /km]	C_{sh} [nF/km]
380 kV	0.025	0.25	13.7

Table 1: Standard overhead line parameters according to [29] for the typical number of cables and wires.

To calculate the line properties the lengths of the transmission lines are needed. As the model of [18] generates an embedded topology, but does not provide a spatial scale, we need an additional step to determine the spatial scale. This is done by requiring that the line lengths of the synthetic grids resemble the line lengths of real EHV grids.

The line lengths l_{mk} in kilometers are obtained by converting the euclidean distances d_{mk} of the lines, which are generated by the random growth model [18]. The conversion factor c is given by the mean length $\langle l \rangle$ of overhead lines in the extra high voltage (EHV) level, that concerns voltages equal or greater than 220 kV, divided by the mean euclidean distance $\langle d \rangle$:

$$c = \frac{\langle l \rangle}{\langle d \rangle} \quad (16)$$

$$l_{mk} = cd_{mk}. \quad (17)$$

Additionally, we used the shortest line l_{min} in the EHV level as a threshold. The admittances of lines that are shorter than l_{min} are set to the threshold impedance of the shortest line.

The mean line length was determined from the *SciGRID* data set [30], which consists of openly available geographic data of the German power grid. At the time of the creation of the data set the coverage of the EHV level in Germany was around 95% [30], which thus offers an excellent basis for such a study.

The *ELMOD* data-set [21] also offers a network topology that is based on network plans by the transmission system operators (TSOs) and OpenStreetMap data. Since the data in *SciGRID* is much better documented and the study deals much more intensively with the network topology, we base our transmission line lengths on *SciGRID*. Still, for completeness, we will also analyze the data from *ELMOD*. A comparison between *SciGRID*, *ELMOD* and our synthetic grids, that are based on *SciGRID* is given in table 2.

	$\langle l \rangle$ [km]	σ_l [km]	l_{min} [km]
<i>SciGRID</i> [30]	37.13	36.59	0.06
<i>ELMOD-DE</i> [21]	40.98	35.54	0.42
Synthetic Grids	37.13	34.6	0.06

Table 2: Comparison of transmission line lengths between different models. The values for the synthetic grid were calculated by generating 10000 different topologies. The mean line length is given by $\langle l \rangle$, the standard deviation of the line length is σ_l and the minimal line length by l_{min} .

In table 2 it can be seen that the mean line length, as well as the standard deviation of the line length of *SciGRID* and *ELMOD*, match well. Furthermore, it can be seen that the synthetic grid line length shows a standard deviation that matches the *SciGRID* as well as the *ELMOD*. The most significant difference between the two data-sets is the minimum line length l_{min} , which is about 4 km in *ELMOD* and about 60 m in *SciGRID*. For the reasons that were stated above, we have adopted l_{min} from *SciGRID*.

Future work would also include not only analyzing the mean and standard deviation of the length but also matching the distributions of line lengths (see fig. 5 in the Appendix). This goes beyond the random growth algorithm [18] which is currently used, and would

require an algorithm that considers line lengths and node locations. A preliminary study [31] on extending the algorithm which uses different node positioning rules has been performed but it does not deal with recovering the correct line length distribution.

2.3.3. Network Models Combining the nodal and line models we obtain the full network model. The power grid topology is given by a graph $\mathcal{G} = \{N, E\}$, where \mathcal{G} is the set of nodes N and edges E [32]. In power systems, the nodes are the buses and the edges are the transmission lines connecting them. The nodal admittance matrix Y is needed to calculate the power flow within the network. It is defined as:

$$Y_{km} = \begin{cases} y_k + \sum_{m=1, k \neq m}^N y_{km} & k = m \\ -y_{km} & k \neq m \end{cases} \quad (18)$$

where y_{km} stands for the admittance between two nodes k, m . The self-admittance of node k is given by y_k and includes all admittances connected to node k [25]. Ohms law defines the current injected at the nodes $I = YU$ and the power flow of the network is given by [33] $S_k = u_k i_k^* = P_k + iQ_k$. Where S_k is the apparent power at node k and P_k and Q_k are the real and reactive power injected at k respectively.

2.4. Operation Point and Reactive Power

Finding an operation point for synthetic power grids is challenging as power systems are generally non-linear and multi-stable. Generally, only the fixed point where all frequencies are synchronous and the voltage magnitudes of all nodes are close to 1 p.u. are physically meaningful for power grids. Furthermore, the AC load flow has no guarantee for convergence and for many synthetic grid models there is no prior information about the reactive power at the nodes.

Reactive power planning is considered to be one of the most intricate problems in power grid planning [34]. The review article [34] gives an excellent overview over the objectives and constraints that are considered in reactive power planning. Instead of implementing one of the complex established models presented in [34] we use a straightforward method to solve the reactive power flow. We employ the voltage stability objective, which is also a standard objective according to [34], and assume that it has to be met perfectly. This requires adjusting the reactive powers at the nodes to match the objective using an ancillary AC power flow. As the synthetic grids generated in this work have less than 10000 nodes our approach still leads to feasible power flow solutions. Once the grids become bigger a more in-depth reactive power flow planning algorithm, such as [35], will be needed to find feasible operation points. The reactive powers of the nodes are adjusted to control the voltage magnitudes in the power grid [25].

To find the nodal reactive powers we generate an ancillary power grid with the same topology, line models and active powers as the full power grid. The ancillary power grid consists purely of PV buses where all nodes are constrained to have voltages magnitudes of $V_m = 1 \text{ p.u.}$ and the same active power that they should generate in the actual power

grid. The reactive powers, of the ancillary grid are found by using the power flow calculation of `PowerModel.jl` [36] and a root-finding algorithm to find a steady state. The operation point of the ancillary grid is used as the initial guess for the operation point search of the actual grid.

2.5. Validators

Real-life power grids are planned carefully to lead to stable operations. Synthetic processes can never fully capture this planning stage. To handle this challenge we will use a rejection sampling approach. Synthetic power grids whose dynamics do not satisfy the stability properties of real-life power grids are rejected. In this section, we will introduce a set of validators that review the stability of the synthetic power grids in their operation point.

The default settings we provide lead to very stable grids, and few or no rejections are observed. Besides their conceptual importance, the practical value of the validators lies in the ability to develop new topological and dynamical models for situations that put more stress on the grid.

To assess our default settings we generated a set of synthetic networks with different sizes and studied the number of rejections. We generated power grids ranging from 100 to 1300 nodes with a step size of 25 nodes. For each grid size we generate 100 power grids and can report that no grid was rejected.

2.5.1. Voltage Magnitude Firstly, we verify that nodal voltages magnitudes full fill the standard of the EN 50160 report [37]. The report specifies that the average 10 minutes root mean square voltage has to stay within the bounds of $\pm 10\%$ for 95% of the week. We assure this by validating that all nodal voltage magnitudes are $V \approx 1p.u.$ in the operation point. If the set-points of the system and the parametrization have been chosen properly the voltage condition should be fulfilled. Even if the reactive power is chosen to ensure a stable power flow with good voltage magnitudes, incorrectly specified control dynamics or machine parameters, can still lead to a violation of the voltage conditions in the operating point. Thus the verification of the voltage condition is still essential in order to catch such mistakes.

2.5.2. Line Loading Stability Margin In a stable operation of the power grid, no line is overloaded. There are different thresholds for the allowed loading of a transmission line. In this work, we will focus on the physically possible limit of the line P_{max} . The power flow transferred over a line connecting node m and k , neglecting the reactive power flow and line losses, is given by:

$$P_{mk} = \frac{V_m V_k}{X_{mk}} \sin(\theta_{mk}) \quad (19)$$

where V_m and V_k are the nodal voltage magnitudes, X_{mk} is the line reactance and θ_{mk} is the difference of the voltage angles of node m and k . The transferred power becomes

maximal when $\theta_{mk} = \frac{\pi}{2}$. Which means that the physically possible limit of the line is $P_{max} = \frac{V_m V_k}{X_{mk}}$. To assure a stable power system transmission lines are operated well below this limit and a so-called stability margin sm is introduced [38]. Which means that the actual transferred power of a line P_{rated} must be below a threshold given by: $P_{rated} \leq P_{max}(1 - sm)$. In this study, we choose $sm = 0.3$ as suggested in [38]. If any line loading in our power grid violates this threshold we reject the power grid.

2.5.3. Small Signal Stability Analysis Since the grids we consider in this work are described by DAEs, we cannot simply study the eigenvalues of the Jacobian in the equilibrium to determine the linear stability of the system. Instead, we perform a small signal stability analysis for DAEs according to [39].

In this approach, the eigenvalues of the so-called reduced Jacobian, or state matrix J_{red} are examined. The reduced Jacobian is set up by decomposing the full Jacobian matrix J into the following blocks:

$$J = \begin{bmatrix} \partial_x f & \partial_y f \\ \partial_x g & \partial_y g \end{bmatrix} \quad (20)$$

where $\partial_x f$ is an abbreviation for the matrix of partial derivatives of the right-hand side of the differential equations f with respect to the differential variables x , and $\partial_y g$ gives the matrix of the partial derivatives of the algebraic equations g with respect to the algebraic variables y .

Following [39], the reduced Jacobian is defined as:

$$J_{red} = \partial_x f - D \quad (21)$$

$$D = \partial_y f (\partial_y g)^{-1} \partial_x g \quad (22)$$

where D is the degradation matrix. The eigenvalues of J_{red} can be examined as usual again, meaning that power grids whose eigenvalues of J_{red} have positive real parts are classified as linearly unstable. Power grids whose operation point is linearly unstable would not exist in reality and therefore have to be rejected before any further investigations are performed.

2.5.4. Probabilistic Capacity Expansion So far we have only assured that the synthetic power grids are stable under a single power set point that was drawn from the probability distribution (4), or any other source. However, real power grids do not operate under a single set point but the set points are rather updated regularly, e.g. in Germany a new demand plan is implanted every 15 minutes. Therefore, it is important to also verify the stability of the grid under different set points. In principle, one can simply run all validators on a sample of set points. In this work, we only focus on the capacity of lines, as this is the most directly affected by the demand, and assure that there is always enough line capacity to cover the expected load cases.

For now, we resort to a simplistic approach and sample completely new set-points from the bimodal distribution (4) but double the mean power P_0 in order to study the system

under more stress. A more realistic analysis of high-stress power flow scenarios would require an extensive investigation of the space of expected set points and is therefore beyond the scope of this paper.

For each new scenario, we calculate the load flow in the grid and then analyze the line loading as given in section 2.5.2. If a line is overloaded we add three additional cables to the line to increase its admittance as in equation (14). This approach is repeated for N different scenarios. So far no new cables were added for all performed simulations. This is to be expected since, for example, in the *SciGRID* [30] data set, more than 90% of the EHV transmission lines have the typical number of cables. It is nevertheless important to validate the grid under different load scenarios to assure its stability. Furthermore, this capacity evaluation could become important once more realistic load scenarios are evaluated, which in the future could include the weather-dependent time series generated by Atlite [23].

While these validators cover the most basic functioning of the grid, further conditions can also be considered. A natural extension for future work would be to add N-1 stability as a condition that the grids need to satisfy.

3. Nodal fluctuations

Due to the increase of the share of variable renewable energy sources (RES), i.e. wind and solar energy, power grids are exposed to new sources of fluctuations. RES are highly fluctuating at different time scales [40, 41] and, particularly, have intermittent fluctuations at short time-scales [42].

Along with supply-side fluctuations, recent studies of high-resolution recorded electricity consumption demonstrate intermittent fluctuations on the demand-side [24, 43, 44] as well. Thus, demand can be another major driver of fluctuations in power grids. To generate synthetic power grids that imitate the dynamics of real power systems at such short time scales, one should add fluctuations from both the supply and demand side to the node models explained in section 2.3.1.

Here we introduce stochastic processes that generate fluctuating wind and solar power, as well as demand time-series. These models have been derived to ensure that, these synthetic time-series have the same short time-scale stochastic characteristics as empirically observed in real data. Therefore, one can confidently use the synthetic time-series for further research in power grids, and consider the response of power systems to these fluctuations. We assume that the nodes with grid forming capabilities can handle the fluctuations internally, but that nodes without grid forming capabilities feed them into the grid. This means we use the synthetic time-series to drive time dependent demand at the PQ-buses. The effects on the grids frequency and voltage are illustrated in section 4.

3.1. Supply fluctuations

The intermittent nature of wind speed and solar irradiance, along with their turbulent-like behavior, which transfer to wind and solar power and, consequently, to power grids has been widely discussed [40, 42, 45, 46]. As demonstrated in these studies, wind and solar power are non-Gaussian time series and, indeed, they have heavy tailed probability distribution function (PDF). Extreme fluctuations, such as a 90% reduction in power in just a few seconds, occur often in RES. These fluctuations can present additional challenges for maintaining the energy balance in power systems. Having a deep insight about the characteristics of RES, and their effects on power grids, allow us to deploy future control strategies that can cope with these extreme fluctuations.

Here, we employ a non-Markovian Langevin-type stochastic process [47], as well as a jump-diffusion model [48] to generate respectively wind and solar power with similar short time-scale characteristics as the empirical data sets. The Langevin-type model used here is:

$$\dot{P}_{wind}(t) = P_{wind}(t)\left(\Gamma - \frac{P_{wind}(t)}{P_0}\right) + \sqrt{\kappa P_{wind}^2(t)}n(t) \quad (23)$$

where, Γ and P_0 are constant parameters, and κ is a parameter with which one can tune the intensity of the noise n (the exact values of these parameters in our simulations are given in Section 4). The noise n is obtained from the following Langevin equation:

$$\dot{n}(t) = -\gamma n(t) + \zeta(t) \quad (24)$$

where ζ is a Gaussian noise with $\langle \zeta(t) \rangle = 0$ and $\langle \zeta(t)\zeta(t') \rangle = \delta(t - t')$. The jump-diffusion model emulating short time-scale fluctuations in the solar power is:

$$dP_{solar}(t) = D^{(1)}(P_{solar}, t)dt + \sqrt{D^{(2)}(P_{solar}, t)}dw(t) + \eta dJ(t) \quad (25)$$

where $D^{(1)}$ and $D^{(2)}$ are respectively the drift and diffusion coefficients. In eq. 25, dw is the Wiener process and dJ is the Poisson process with jump size η , which is assumed to be a normally distributed random number, i.e. $\eta \sim N(0, \sigma_\eta)$. The Poisson process comprises also a jump rate, which we call λ . The advantage of the jump-diffusion model is that it is a non-parametric model, i.e. all parameters are derived from the empirical data sets (for more details see [48]).

3.2. Demand fluctuations

Standard load profiles used to balance energy in the grid in advance have a time resolution of 15 minutes. Shorter time scales are balanced by control mechanisms rather than by trading. To study the dynamics at short time scales the load profiles are thus of limited use. Instead we can consider empirical measurements of loads that have a high enough resolution to reveal short term fluctuations such as [24, 43, 49].

Here, we apply the superstatistics model introduced in [24] to generate the short time-scales fluctuations of the demand-side and add them to the dynamic model of load in

PQ-bus. Following the superstatistical approach the demand fluctuations are obtained by taking the 2-norm of several Gaussian distributions plus a constant offset μ_{MB} :

$$P^{fluc}(t) = \sqrt{(z_1(t))^2 + (z_2(t))^2 + \dots + (z_J(t))^2} + \mu_{MB} \quad (26)$$

where we use $J = 3$ as discussed in [24], and $z_i(t)$ is obtained from the following Langevin equation:

$$dz_i(t) = \gamma z_i(t)dt + \epsilon dw_i \quad (27)$$

where dw_i is the Wiener process with a mean 0 and standard deviation $\sigma = \epsilon/\sqrt{2\gamma}$. We employ the same parameter values μ_{MB} , γ , and ϵ as reported in [24].

It should be noted that the stochastic time series we have introduced here are based on empirical measurements of power grid actors that are typically not directly connected to the highest level of the power grid. As not all producers and consumers connected to a particular bus are perfectly correlated the fluctuations would be somewhat attenuated in reality. Unfortunately few or no measurements of the actual correlations of fluctuations exist, and we have to leave this point to future work.

4. Simulation Examples

In this section we generate a fully electrified synthetic power grid, whose structure is shown in figure 2, and will study its behavior in response to the three different fluctuations processes that have been introduced in section 3. The synthetic grid that we consider here consists of 100 nodes with an equal share of grid following and grid forming inverters. We expect that future power grids will have a high share of variable renewable energies and, therefore, we consider multi-node fluctuations in this example. We assume that the grid-forming inverters are equipped with sufficiently large storage units. Hence the RES fluctuations are only fed into the grid via the grid-following inverters.

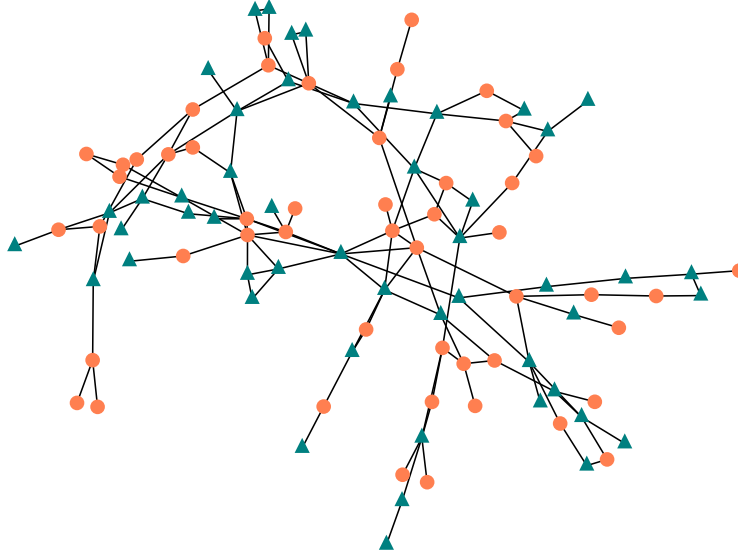


Figure 2: Network structure of a synthetic power grid. Triangular and circular nodes depict grid-following and grid forming inverters respectively.

The fluctuations $P_{fluc,i}(t)$ are added to the set points $P_{set,i}$ of the nodes. This results in the following equation for the active power P_i at node i :

$$P_i(t) = P_{set,i} + P_{fluc,i}(t). \quad (28)$$

For the different processes we will analyze the two edge cases, completely correlated fluctuations, meaning that all nodes have the same fluctuating time series $P_{fluc}(t)$, and secondly completely uncorrelated fluctuations where all nodes have different fluctuating time series.

In order to compare the results we will study two performance measures, the synchronization norm $\|\mathcal{L}\|_{sync}$ [50] and the L_2 norm of the average deviation from the nominal grid frequency $\|\mathcal{L}\|_{dev}$ [51]:

$$\|\mathcal{L}\|_{sync} = \sqrt{\frac{1}{T} \int_0^T \frac{1}{N} \sum_{m=1}^N \left(\omega_m(t) - \frac{1}{N} \sum_{k=1}^N \omega_k(t) \right)^2 dt} \quad (29)$$

$$\|\mathcal{L}\|_{dev} = \sqrt{\frac{1}{T} \int_0^T \frac{1}{N} \sum_{m=1}^N (\omega_m(t) - \omega_0)^2 dt} \quad (30)$$

where ω_0 is the nominal grid frequency. The indices m, k run over all N grid-forming inverters as the grid-following inverters have no internal frequency dynamics (7).

The synchronization norm (29) measures the synchronicity in the power grid. A large synchronization norm expresses a lack of synchronization. The synchronization norm however neglects any fluctuation of the so-called bulk [52], the joint response of the

entire power grid, of synchronous frequencies. Therefore the authors of [51] introduce the deviation norm $||\mathcal{L}||_{dev}$ which measures the contribution of the bulk to the fluctuations. In [51] it has been shown that the bulk is the dominant contributor in response to single node renewable energy fluctuations.

The results are summarized in table 3 and 4. In all cases it can be seen that the deviation norm $||\mathcal{L}||_{dev}$ is larger than the synchronization norm. This indicates that the bulk fluctuations are the main contributors for multi-node renewable energy fluctuations as well. This holds for all fluctuation process and for both edge cases, the correlated or uncorrelated fluctuations. Furthermore, we can see that the deviation norm is smaller for the uncorrelated case than for the correlated case, which is to be expected. Moreover it can be seen that the synchronization norm is very small for all cases which implies that the networks have a high degree of synchronicity under renewable energy fluctuations.

	$ \mathcal{L} _{sync}$	$ \mathcal{L} _{dev}$ [51]
Wind Fluctuations	0.001	0.874
Demand Fluctuations	0.002	1.952
Solar Fluctuations	0.033	0.686

Table 3: Performance measures for completely correlated fluctuations.

	$ \mathcal{L} _{sync}$	$ \mathcal{L} _{dev}$ [51]
Wind Fluctuations	0.001	0.153
Demand Fluctuations	0.002	0.417
Solar Fluctuations	0.027	0.099

Table 4: Performance measures for completely uncorrelated fluctuations.

In the following we will go more into more details for the results of the demand fluctuations. The results for the solar and wind fluctuations can be found in the appendix 5.

The figures 3 and 4 show the results for the correlated and uncorrelated demand fluctuations respectively. In this example we use the coefficients for the stochastic process, introduced in [24], which have been extracted from the NOVAREF data set [53] which consists of high-resolution demand profiles. In a transmission grid, the number of consumers is significantly higher than in the data-sets analyzed in [24]. We expect that the fluctuations that take place at a single node will average out to some extent because the demand of all consumers is not fully correlated. The actual fluctuations should therefore be smaller. Thus, the result which we present here should be considered a pessimistic estimate. This explains why the frequency response for the uncorrelated fluctuations shown in figure is relatively severe and occasionally even surpasses 0.1 Hz. For all fluctuation processes considered in this work we find that the voltage magnitudes

of the nodes stay close to the set-point of 1 [p.u.] which is to be expected as we simulate active power fluctuations which couple to the frequency.

This example demonstrates that we are able to generate robust and stable synthetic grids. The grid does not lose synchrony even under fluctuations which are stronger than they will be in reality as we have not considered averaging effects at the nodes.

This opens the door to future research that studies grids that are under severe stress, possibly from compound events, meaning that multiple stressors occur at once. Extreme scenarios that can destabilize grids include the loss of multiple lines, as grids are built N-1 stable, special weather conditions that can cause storage to be locally depleted, causing grid forming inverters to have to compromise on their grid forming capabilities and to inject fluctuations as well.

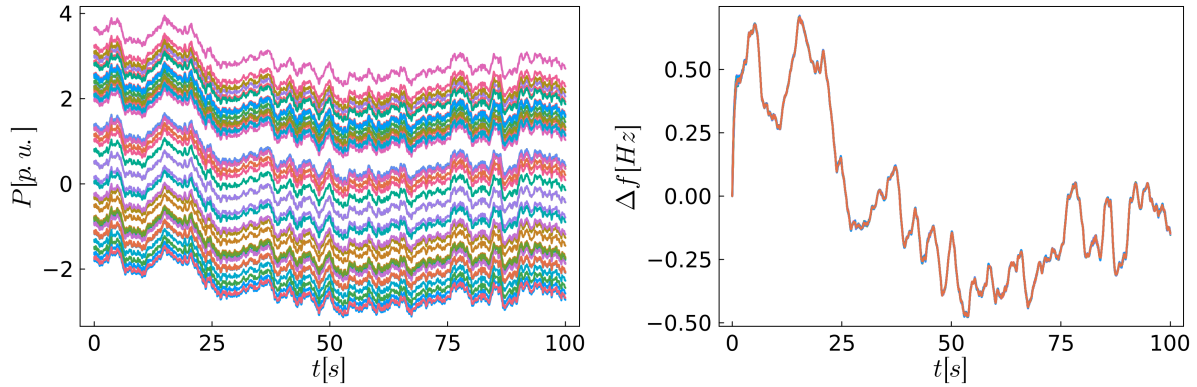


Figure 3: Results for completely correlated demand fluctuations at the nodes. Figure on the left shows the active powers of the grid-following inverters. The frequency response of the grid-forming inverters is shown in the figure on the right side. The parameters $[\gamma, \epsilon, \mu_{MB}] = [0.016, 33.81, 0.03]$, as in [24], were used to generate the demand fluctuations.

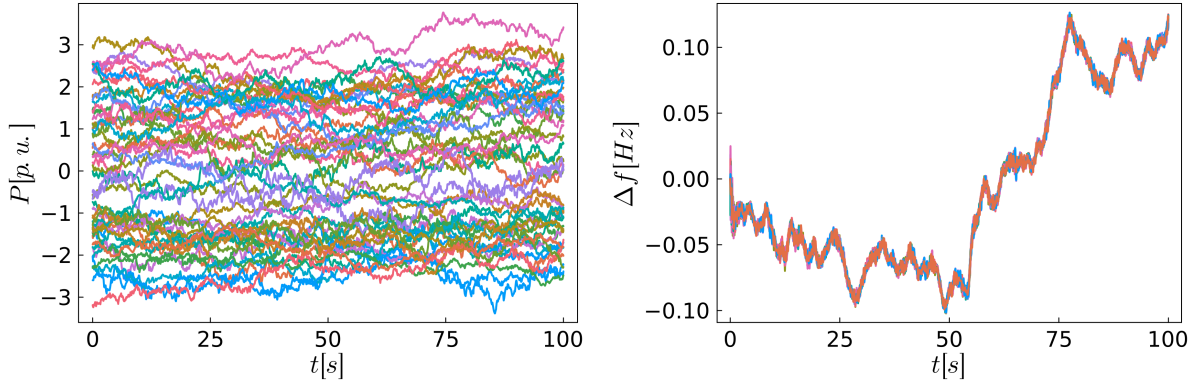


Figure 4: Results for completely uncorrelated demand fluctuations at the nodes. Figure on the left shows the active powers of the grid-following inverters. The frequency response of the grid-forming inverters is shown in the figure on the right side. The parameters $[\gamma, \epsilon, \mu_{MB}] = [0.016, 33.81, 0.03]$, as in [24], were used to generate the demand fluctuations.

5. Conclusions

In this work a framework to generate synthetic power grid models for studying collective dynamical effects has been introduced. For the first time the following established methods are combined to obtain synthetic power grids: topologies [18], active power set-points [21, 22] and short term fluctuations, node [17] and line models and finally an operation point that is validated to fulfill certain stability criteria [38, 45]. Each element in the framework can be substitute as long as it adheres to the general structure thus making the approach modular. For the default elements we have chosen methods which have already been used in various research projects. We have reviewed these established approaches and are drawing attention to possible improvements in the respective sections, in particular in order to investigate electricity grids with a high share of renewable energy. In particular, we have identified two elements that need improvement, the generation of network topologies and the distribution of active power supply.

An essential contribution of this work is a set of validators that ensure that the different parts of the system work well together to provide a plausible stable operating state. This will be a key technical tool for developing new models in the future.

The topologies created with the random growth model [18] cannot reflect the distribution of transmission line lengths in the empirical *SciGRID* data-set [30]. The model has been designed to resemble network properties, such as the degree distribution, of real EHV power grids. However, the positioning of the nodes is random, which does not reflect the growth of power grids realistically. We assume that it is possible to correct the length distribution by introducing an additional step in the algorithm that considers the geographical location of the nodes. Furthermore, we have assumed that the transmission system topology will remain very similar to today's. Future studies should consider how

the energy transition influences the topology, as for example, RES are connected to the grid differently than large power plants and the grid evolves to adapt to the new locations.

The major issue in the distribution of active power supply for our synthetic model is that the *ELMOD-DE* [21] specifies scenarios which reflect the current power supply. As we are interested in studying future dynamics as well, a new method for drawing active power is needed. Atlite [23] is a software tool that generates weather dependent power generation potentials and time series for renewable energy technologies. These potentials and time series are a promising tools that could be used to update the active power supply in our model. Further, as the time-series depend on the weather, they could also be used to study the synthetic grid under multiple supply scenarios.

Besides the generation of the synthetic grid dynamics in stable operation points, we also include the major drivers of fluctuations at short time scales. We have implemented the three major drivers of short term fluctuations in future power grids, solar, wind and demand. As an example we study a fully synthetic power grid under these fluctuations. We have decided to add the fluctuations only to the components without grid-forming capabilities as grid-forming components will usually be equipped with sufficient storage. We find that the synthetic grid shows good synchronicity under all three fluctuation scenarios. We saw that there is a relevant contribution of the joint response of synchronous frequencies.

It remains a challenge to find a balance between simplicity and tractability of the model and realism. We have outlined a wide range of points at which realism can be increased. In the current state the complete model is already well suited to drive new research directions. This includes developing methods to study compound and extreme events that particularly stress the system. More immediately it will allow us to advance the study of dynamic power grid stability using graph neural networks [9,13,14]. It enables for the first time to generate a large and robust set of heterogeneous DAE models that will challenge the GNN models in completely new ways, and allow us to take one step closer to predicting the dynamic stability of real power grids.

References

- [1] Athay T, Podmore R and Virmani S 1979 *IEEE Transactions on Power Apparatus and Systems* 573–584
- [2] Grigg C, Wong P, Albrecht P, Allan R, Bhavaraju M, Billinton R, Chen Q, Fong C, Haddad S, Kuruganty S *et al.* 1999 *IEEE Transactions on power systems* **14** 1010–1020
- [3] Birchfield A B, Gegner K M, Xu T, Shetye K S and Overbye T J 2017 *IEEE Transactions on Power Systems*
- [4] Birchfield A B, Xu T, Gegner K M, Shetye K S and Overbye T J 2017 *IEEE Transactions on Power Systems*
- [5] Xu T, Birchfield A B, Shetye K S and Overbye T J 2017 Creation of synthetic electric grid models for transient stability studies *The 10th Bulk Power Systems Dynamics and Control Symposium (IREP 2017)*

- [6] Höfllich B, Richard P, Völker J, Rehtanz C, Greve M, Gwisdorf B, Kays J, Noll T, Schwippe J, Seack A *et al.* 2012 *Deutsche Energie-Agentur, Berlin Germany*
- [7] Amme J, Pleßmann G, Bühler J, Hülk L, Kötter E and Schwaegerl P 2018 *Journal of Physics: Conference Series*
- [8] Che Y and Cheng C 2021 *Chaos: An Interdisciplinary Journal of Nonlinear Science* **31** 053129
- [9] Nauck C, Lindner M, Schürholt K, Zhang H, Schultz P, Kurths J, Isenhardt I and Hellmann F 2022 *New Journal of Physics* **24** 043041
- [10] Menck P J, Heitzig J, Kurths J and Joachim Schellnhuber H 2014 *Nature communications* **5** 1–8
- [11] Schultz P, Heitzig J and Kurths J 2014 *New Journal of Physics* **16** 125001
- [12] Nitzbon J, Schultz P, Heitzig J, Kurths J and Hellmann F 2017 *New Journal of Physics* **19** 033029
- [13] Nauck C, Lindner M, Schürholt K and Hellmann F 2022 *arXiv preprint arXiv:2206.06369*
- [14] Nauck C, Lindner M, Schürholt K and Hellmann F 2022 Towards dynamical stability analysis of sustainable power grids using graph neural networks accepted at NeurIPS 2022
- [15] Christensen P, Andersen G K, Seidel M, Bolik S, Engelken S, Knueppel T, Krontiris A, Wuerflinger K, Bülo T, Jahn J *et al.* 2020 High penetration of power electronic interfaced power sources and the potential contribution of grid forming converters
- [16] Witthaut D, Hellmann F, Kurths J, Kettemann S, Meyer-Ortmanns H and Timme M 2022 *Rev. Mod. Phys.* **94**(1) 015005 URL <https://link.aps.org/doi/10.1103/RevModPhys.94.015005>
- [17] Kogler R, Plietzsch A, Schultz P and Hellmann F 2022 *PRX Energy* Publisher: American Physical Society
- [18] Schultz P, Heitzig J and Kurths J 2014 *The European Physical Journal Special Topics* **223**
- [19] ENTSO-E 2020 Ten-year network development plan 2020 – main report URL https://consultations.entsoe.eu/system-development/tyndp2020/consult_view/
- [20] Brown T, Schlachtberger D, Kies A, Schramm S and Greiner M 2018 *Energy* **160** 720–739
- [21] Egerer J 2016 Open source electricity model for germany (elmod-de) Tech. rep. DIW Data Documentation URL <http://hdl.handle.net/10419/129782>
- [22] Taher H, Olmi S and Schöll E 2019 *Physical Review E* **100** 062306
- [23] Hofmann F, Hampp J, Neumann F, Brown T and Hörsch J 2021 *Journal of Open Source Software* **6** 3294 URL <https://doi.org/10.21105/joss.03294>
- [24] Anvari M, Proedrou E, Schäfer B, Beck C, Kantz H and Timme M 2022 *Nature communications* **13** 1–12
- [25] J Machowski J J Bialek J B 2008 *Power System Dynamics - Stability and Control* (Wiley & Sons)
- [26] Schiffer J, Ortega R, Astolfi A, Raisch J and Sezi T 2014 *Automatica*
- [27] Schmietendorf K, Peinke J, Friedrich R and Kamps O 2014 *Eur. Phys. J. Spec. Top.* **223** 2577–2592
- [28] Andersson G 2012 Power system analysis ETH Zürich: Lecture 227-0526-00 Script
- [29] dena 2012 dena-Verteilnetzstudie: Ausbau- und Innovationsbedarf der Stromverteilnetze in Deutschland bis 2030 URL <https://www.dena.de/newsroom/publikationsdetailansicht/pub/dena-verteilnetzstudie-ausbau-und-innovationsbedarf-der-stromverteilnetze-in-deutschland-bis-2030>
- [30] Medjroubi W, Müller U P, Scharf M, Matke C and Kleinhans D 2017 *Energy Reports* **3** URL <https://www.sciencedirect.com/science/article/pii/S2352484716300877>
- [31] Schultz P, Hellmann F, Heitzig J and Kurths J 2017 A network of networks approach to interconnected power grids URL <https://arxiv.org/abs/1701.06968>
- [32] Newman M 2010 *Networks. An Introduction* (Oxford University Press)
- [33] J J M, Bialek J and Bumby J 2008 *Power System Dynamics - Stability and Control* (Wiley & Sons)
- [34] Zhang W, Li F and Tolbert L M 2007 *IEEE Transactions on Power Systems* **22**(4) 2177 – 2186
- [35] Birchfield A B, Xu T and Overbye T J 2018 *IEEE Transactions on Power Systems* **33** 6667–6674
- [36] Coffrin C, Bent R, Sundar K, Ng Y and Lubin M 2018 Powermodels.jl: An open-source framework for exploring power flow formulations 2018 *Power Systems Computation Conference (PSCC)* pp

1–8

- [37] Standardization E C F E 2011 En 50160: Voltage characteristics of electricity supplied by public distribution systems
- [38] Gonen T 2014 *Electrical Power Transmission System Engineering: Analysis and Design* (CRC Press) ISBN 9781482232226
- [39] Milano F 2010 *Power System Modelling and Scripting* Power Systems (Springer)
- [40] Apt J 2007 *Journal of Power Sources* **169** 369–374
- [41] Woyte A, Belmans R and Nijs J 2007 *Solar Energy* **81** 195–206
- [42] Anvari M, Lohmann G, Wächter M, Milan P, Lorenz E, Heinemann D, Tabar M R R and Peinke J 2016 *New Journal of Physics* **18** 063027
- [43] Wright A and Firth S 2007 *Applied Energy* **84** 389–403
- [44] Monacchi A, Egarter D, Elmenreich W, D’Alessandro S and Tonello A M 2014 Greend: An energy consumption dataset of households in italy and austria *2014 IEEE International Conference on Smart Grid Communications (SmartGridComm)* (IEEE) pp 511–516
- [45] Milan P, Wächter M and Peinke J 2013 *Physical review letters* **110** 138701
- [46] Curtright A E and Apt J 2008 *Progress in Photovoltaics: Research and Applications* **16** 241–247
- [47] Schmietendorf K, Peinke J and Kamps O 2017 *The European Physical Journal B* **90** 1–6
- [48] Anvari M, Werther B, Lohmann G, Wächter M, Peinke J and Beck H P 2017 *Solar Energy* **157** 735–743
- [49] Marszal-Pomianowska A, Heiselberg P and Larsen O K 2016 *Energy* **103** 487 – 501 ISSN 0360-5442
- [50] Andreasson M, Tegling E, Sandberg H and Johansson K H 2017 Coherence in synchronizing power networks with distributed integral control *2017 IEEE 56th Annual Conference on Decision and Control (CDC)* (IEEE) pp 6327–6333
- [51] Plietzsch A, Auer S, Kurths J and Hellmann F 2019 Linear response theory for renewable fluctuations in power grids with transmission losses URL <https://arxiv.org/abs/1903.09585>
- [52] Zhang X, Hallerberg S, Matthiae M, Witthaut D and Timme M 2019 *Science advances* **5** eaav1027
- [53] Lange M and Zobel M 2016 Novaref, erstellung neuer referenzlastprofile zur auslegung, dimensionierung und wirtschaftlichkeitsberechnung von hausenergieversorgungssystemen, tech. rep.

Appendix

Line Length Distribution

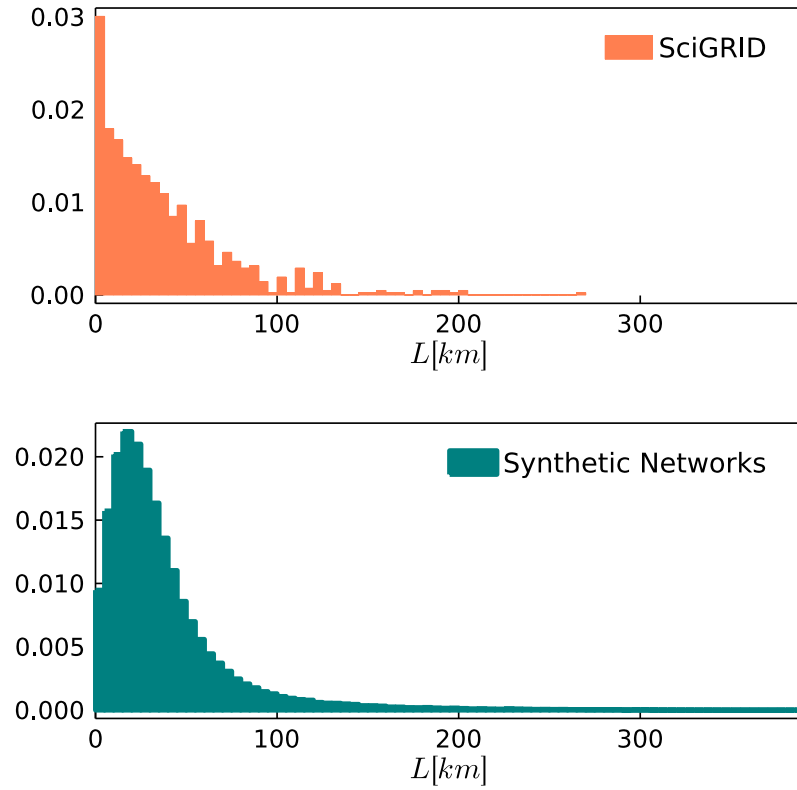


Figure 5: Histograms of the line lengths in the *SciGRID* data set [30] and of our synthetic model. Both distributions show heavy tails. The data for the *SciGRID* lines indicates a scale-free distribution but the quantity of data is too small to make accurate statements. Further investigations are necessary.

RES Fluctuation Examples

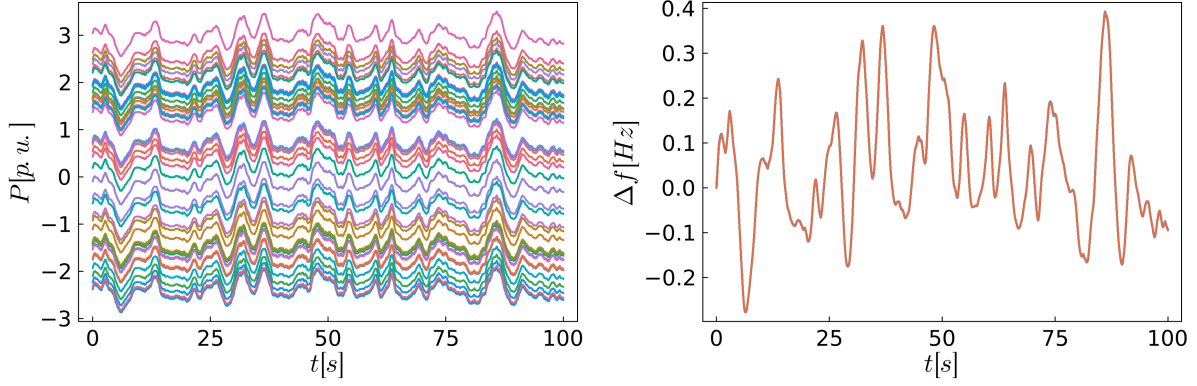


Figure 6: Results for completely correlated wind power fluctuations. The parameters $[D, \gamma, g, \epsilon] = [0.1, 1.0, 0.5, 1.0]$, as in [47], were used to generate the wind power fluctuations.

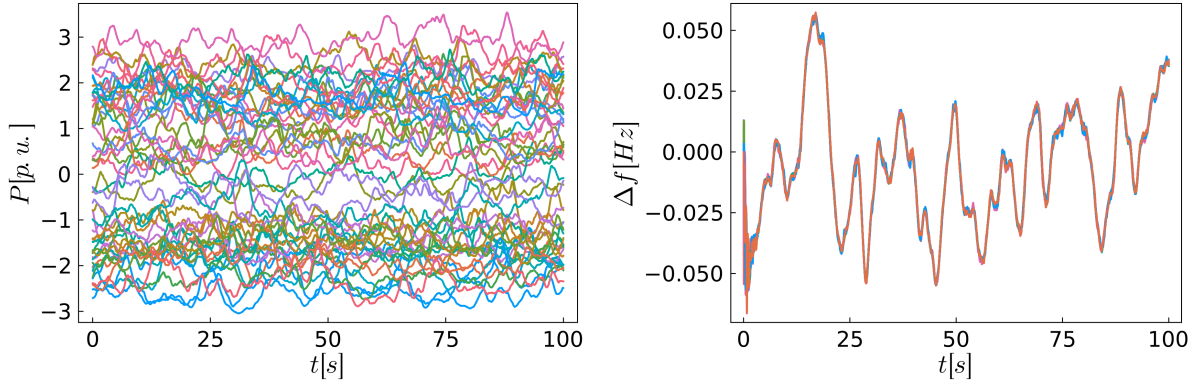


Figure 7: Results for completely uncorrelated wind power fluctuations. The parameters $[D, \gamma, g, \epsilon] = [0.1, 1.0, 0.5, 1.0]$, as in [47], were used to generate the wind power fluctuations.

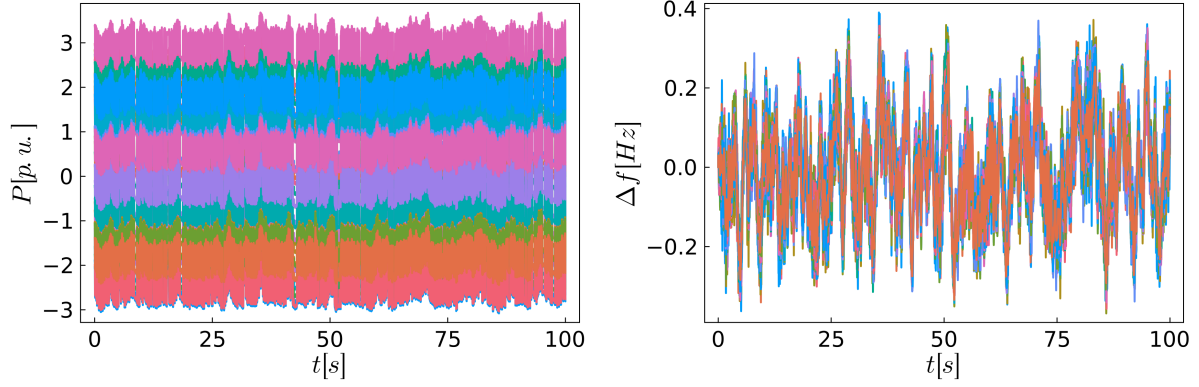


Figure 8: Results for completely correlated solar power fluctuations. The parameters $[D^{(2)}, \lambda, \sigma_\eta] = [0.001, 0.01, 0.02]$, as in [48], were used to generate the solar power fluctuations.

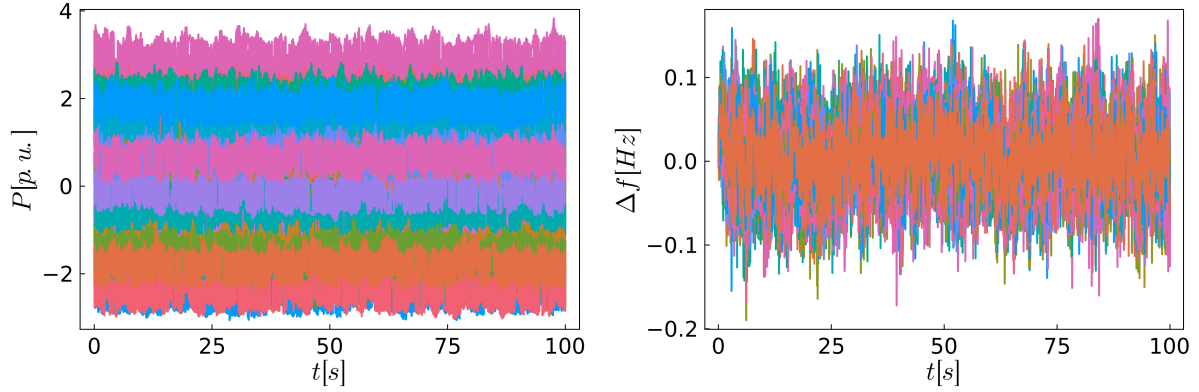


Figure 9: Results for completely uncorrelated solar power fluctuations. The parameters $[D^{(2)}, \lambda, \sigma_\eta] = [0.001, 0.01, 0.02]$, as in [48], were used to generate the solar power fluctuations.